View metadata, citation and similar papers at core.ac.uk
brought to you by CORE
provided by CERN Document Server

An X-ray Nebula Associated with the Millisecond Pulsar B1957+20

B. W. Stappers,[1,2*] B. M. Gaensler,[3] V. M. Kaspi,[4,5]
M. van der Klis,[2] W. H. G. Lewin,[5]

[1]Stichting ASTRON, 7990 Dwingeloo, The Netherlands

[2]Sterrenkundig Instituut "Anton Pannekoek",1098 SJ Amsterdam, The Netherlands

[3]Harvard-Smithsonian Center for Astrophysics,60 Garden St, Cambridge, Massachusetts, USA

[4]Physics Department, McGill University,3600 University Street, Montreal, Quebec, Canada

[5]Physics Department and Center for Space Research,Massachusetts Institute of Technology, 70 Vasser St., Cambridge, Massachusetts, USA

*To whom correspondence should be addressed; E-mail: stappers@astron.nl

We have detected an x-ray nebula around the binary millisecond pulsar B1957+20. A narrow tail, corresponding to the shocked pulsar wind, is seen interior to the known Hα bow shock and proves the long-held assumption that the rotational energy of millisecond pulsars is dissipated through relativistic winds. Unresolved x-ray emission likely represents the shock where the winds of the pulsar and its companion collide. This emission indicates that the efficiency with which relativistic particles are accelerated in the post shock flow is similar to that for young pulsars, despite the shock proximity and much weaker surface magnetic field of this millisecond pulsar.

Millisecond pulsars are old neutron stars (typically $\sim 3\,$Gyr) that have been spun up to a rapid rotation rate ($\lesssim 25\,$ms) by accretion of material from a binary companion (*1*, *2*). After the

accretion phase, they appear as radio pulsars with surface magnetic field strengths of $\sim 10^8$ G, which, combined with their older ages and rapid rotation rates, means that they form a separate population from younger pulsars.

PSR B1957+20 is the second fastest-spinning pulsar known, with a rotation period (*3*) of 1.6 ms and rotational spin-down luminosity (*4*) $\dot{E} = 1 \times 10^{35}$ ergs s^{-1}. The pulsar is in a 9.16-hour binary orbit with a low-mass companion star. The wind of the companion star eclipses the radio emission for $\sim$10% of every orbit. The PSR B1957+20 binary system provides an excellent opportunity to study the wind of a weakly magnetized, recycled neutron star. The wind is ablating, and may eventually evaporate, the low-mass companion star. Ablation and heating of the companion star (*5*) are believed to be caused by x- or γ-rays generated in an intrabinary shock between the pulsar wind and that of the companion star. Meanwhile, the high space velocity of the pulsar (> 220 km s^{-1}) (*6*), as it moves through the interstellar medium (ISM), generates sufficient ram-pressure to confine the pulsar wind and results in the formation of a bow shock. Upstream of this bow shock Hα emission is generated where neutral material is swept up and collisionally excited; this Hα nebula absorbs 1–10% of the spin-down energy (*7*). A reverse or termination shock decelerates the pulsar wind and is located between the pulsar and the bow shock.

The intrabinary and termination shocks both provide diagnostics of the pulsar wind. Observations of the interaction of young pulsar winds and the ISM have shown that they power x-ray emitting synchrotron nebulae which are typified by the Crab nebula (*8*). High-resolution observations of such pulsar-wind nebulae have shown that the composition of the wind, characterized by the ratio of the Poynting flux to particle energy flux σ, is kinetic energy dominated ($\sigma \approx 0.003$). However, for the evolutionarily distinct millisecond pulsar population, the composition, efficiency, and geometry of the pulsar wind remain unknown. *ROSAT* observations of PSR B1957+20 provided the only previous constraint, and they have been interpreted as indi-

cating that its wind is different from that of the Crab pulsar (*9*). However, these data lacked the spatial resolution and sensitivity to determine the cause of the emission.

We have undertaken a 43 kilosecond (*10*) observation of the millisecond pulsar B1957+20 using the *Chandra* X-ray Observatory. The brightest x-ray source in the field (Fig. 1) is coincident with the pulsar position. A tail of x-ray emission is seen extending from the pulsar to the northeast by at least 16″ with a position angle opposite to the pulsar's proper motion direction of 212° (*6*).

Striking confirmation of the association with the pulsar and the ISM shock comes by comparing this x-ray tail with the Hα bow-shock nebula (Fig. 2). In bow-shock nebulae, material at the termination shock is swept back by the ram pressure and forms a cylindrical tube aligned with the proper motion direction and interior to the bow shock (*13, 14*). The morphology, direction and location of the x-ray nebula (Fig. 2) therefore indicate that it corresponds to the termination shock and, in combination with the enclosing Hα emission, demonstrates the expected double-shock nature of the pulsar's interaction with the ambient medium.

Young pulsar winds are thought to be relativistic, and correspondingly generate non-thermal emission by synchrotron and/or inverse Compton processes (*15,16*). However, nothing is known about millisecond pulsar winds except that the scale of the observed Hα nebulae are at least consistent with their having relativistic winds (*17*). A different wind might be expected because of the reduction and possible alteration of the nature of the magnetic field during the accretion phase. We must therefore also consider the possibility that they drive slower winds like that of the Sun, resulting in shock-heated thermal x-rays. If the spin-down luminosity of a millisecond pulsar is carried away as kinetic energy in an outflow then $\dot{E} = 0.5\dot{M}V_w^2$, where $\dot{M}$ is the mass loss rate and V_w is the wind speed. Because the pulsar remains and is at least 1 Gyr old we know that $\dot{M} < 10^{17}\,\mathrm{g\,s^{-1}}$, and thus $V_w > 10^9\,\mathrm{cm\,s^{-1}}$. The temperature that we measure ($kT \approx 1$ keV, where k is the Boltzmann constant) by fitting a spectrum expected for shock-heated gas to the

energy distribution of the 82 counts recorded in the tail region is inconsistent with such high velocities (*18*).

The emission must therefore be from some form of non thermal process, either synchrotron or inverse Compton emission, as seen in wind nebulae around young pulsars. In either case, the x-ray emission requires a population of relativistic particles in the pulsar wind. Thus, the detection of a distinct x-ray tail provides direct evidence that millisecond pulsars lose their rotational energy through relativistic winds.

It is highly unlikely that diffuse shock acceleration (*19*) is the mechanism that generates the emitting particle population in this nebula, because it is difficult to accelerate particles in a relativistic flow through this mechanism (*20*). As in other pulsar wind nebulae, the acceleration presumably takes place through some other mechanism possibly involving the role of heavy ions (*21*)

Because the pulsar and the companion are separated by only 1.5×10^{11} cm, the intrabinary shock, formed where the pulsar and companion winds interact, will be located in a strong magnetic field (much stronger than that at the shock in the Crab nebula). This intrabinary shock is therefore a potential source of unresolved synchrotron emission at the location of the pulsar (*22*) and can be used to determine the wind characteristics at the shock front. The x-ray luminosity in the shock is dependent on both the post shock magnetic field strength and σ (*8*). We therefore consider two possibilities for the wind composition of PSR B1957+20: either dominated by kinetic energy ($\sigma = 0.003$ as seen in the Crab nebula) or magnetically dominated ($\sigma \gg 1$). We can describe the process by which the spin-down energy of the pulsar is converted into x-ray emission at the intrabinary shock by (*9*):

$$f_b \Delta\varepsilon L_\varepsilon = f_{rad} f_\gamma f_{geom} \dot{E} \tag{1}$$

where L_ε is the spectral x-ray luminosity in a band of width $\Delta\varepsilon \approx 1$ keV centered on a pho-

ton energy $\varepsilon = 1\,\mathrm{keV}$. The geometric factor f_{geom} defines how much of the wind interacts with the companion, f_γ is the fraction of the intercepted spin-down energy flux that goes into accelerating electrons with Lorentz factor γ corresponding to $\varepsilon = 1\,\mathrm{keV}$, and f_{rad} is the radiative efficiency of the corresponding synchrotron emission. The fraction of the unresolved x-ray emission that is due to synchrotron emission produced at the intrabinary shock is f_b, the remainder presumably being emission produced by the pulsar itself.

Table 1: Properties of the PSR B1957+20 system (*6*), and comparison with the Crab nebula and its central pulsar (*23*). The fraction of the wind of PSR B1957+20 that interacts with the companion star wind is $f_{geom} \gtrsim r_e^2/(4a^2) \approx 0.02$, where a is the orbital separation. This fraction is a lower limit, because the pulsar wind is most likely focused into the equatorial plane (*24,25*) which is also probably the orbital plane of the binary system (*2*). The companion star would therefore intercept more of the spin-down energy from the pulsar than if it has a spherical wind.

Parameter	B1957+20		Crab
	($\sigma = 0.003$)	($\sigma \gg 1$)	Nebula / pulsar
Spin period (ms)	1.6		33.5
Surface magnetic field (10^8 G)	1.4		3.8×10^4
Distance (kpc)	1.5		2
Age (yr)	$> 2 \times 10^9$		948
Distance to shock (cm)	$\sim 1.5 \times 10^{11}$		$\sim 3 \times 10^{17}$
$\dot{E}$ (10^{35} erg s^{-1})	1.0		4.4×10^3
f_b	~ 0.5		...
f_{geom}	$\gtrsim 0.02$		...
B (G)	2	12	$\approx 10^{-4}$
t_{flow} (s)	5	1.7	$\sim 3 \times 10^{10}$
t_{rad} (s)	700	45	$\sim 5 \times 10^{11}$
f_{rad}	0.007	0.04	0.06
ε ($\gamma \approx 10^5$)	1 keV		70 μm
L_ε ($\gamma \approx 10^5$) (erg s^{-1} keV^{-1})	2.6×10^{30}		5.8×10^{40}
f_γ ($\gamma \approx 10^5$)	< 0.09	< 0.02	0.04

The flow immediately downstream of the intrabinary shock is expected to undergo Doppler

boosting as it passes around the companion (*22*). Thus, one expects the x-ray emission at orbital phases before and after eclipse to be enhanced by up to a factor 2.2 depending on the flow speed and the degree of absorption and/or scattering by the companion wind (*22*). In contrast, the x-ray emission at the eclipse (orbital phase 0.25) may be reduced because of obscuration of the shock by the companion star. If we can measure these variations then we can determine f_b. The lowest and highest count rates in the folded light curve (Fig 3.) are during and immediately after eclipse, respectively, with comparatively low probability of this variation being by chance (see caption of Fig 3.). If this apparent orbital modulation is genuine and corresponds to a modulation of the x-ray flux from the intrabinary shock by a factor of 2.2, then we find that $f_b \sim 0.5$.

The post shock magnetic field strengths (*8*) corresponding to our two limiting values of σ (0.003 and $\gg 1$) are listed in Table 1; the corresponding Lorentz factors of the synchrotron emitting relativistic electrons for both cases are $\gamma = 2.4 \times 10^5 (\varepsilon/B)^{1/2} \approx 10^5$ at $\varepsilon = 1\,$keV, where B is the post shock magnetic field strength. For each case the emitting region is taken to be the radius of the radio-eclipse region (*6*) $r_e = 5 \times 10^{10}\,$cm; for $\sigma = 0.003$ the flow speed is $v_{flow} = c/3$, whereas for $\sigma \gg 1$ we expect $v_{flow} = c$ (*8*). The corresponding residence times are given by $t_{flow} = v_{flow}/r_e$ (Table 1), and the radiative lifetimes of the emitting electrons are $t_{rad} = 5.1 \times 10^8/(\gamma B^2)$. We can thus compute the radiative efficiency (*26*) in each case as $f_{rad} = (1 + t_{rad}/t_{flow})^{-1}$. With $f_{geom} > 0.02$ (Table 1) and $f_b \sim 0.5$, we can infer that $f_\gamma < 0.09$ ($\sigma = 0.003$) or $f_\gamma < 0.02$ ($\sigma \gg 1$) for Lorentz factor $\gamma \sim 10^5$.

We directly compared the properties of the shocked wind of PSR B1957+20 with those derived for the Crab nebula with the same Lorentz factor and find that $f_\gamma \approx 0.04$ for electrons with $\gamma = 10^5$ in the Crab, which, regardless of the assumed value of σ, is similar to that which we derived for PSR B1957+20. The available evidence therefore suggests that despite being subject to a prolonged evolutionary process that has altered its magnetic field by many orders

of magnitude and having a shock that occurs much closer to the pulsar, this millisecond pulsar generates a wind for which the efficiency of relativistic particle acceleration in this post shock flow is similar to that seen for the winds of young pulsars. New *Chandra* data on this and other pulsars (*27–29*) are providing the first detailed observational input into studies of relativistic flows, particle acceleration, and magnetohydrodynamic shocks.

References and Notes

1. M. A. Alpar, A. F. Cheng, M. A. Ruderman, J. Shaham, *Nature* **300**, 728 (1982).
2. D. Bhattacharya, E. P. J. van den Heuvel, *Phys. Rep.* **203**, 1 (1991).
3. A. S. Fruchter, D. R. Stinebring, J. H. Taylor, *Nature* **333**, 237 (1988).
4. M. Toscano, *et al.*, *Mon. Not. R. Astron. Soc.* **307**, 925 (1999).
5. A. S. Fruchter, J. Bookbinder, C. Bailyn, *Astrophys. J.* **443**, L21 (1995).
6. Z. Arzoumanian, A. S. Fruchter, J. H. Taylor, *Astrophys. J.* **426**, L85 (1994).
7. S. R. Kulkarni, J. J. Hester, *Nature* **335**, 801 (1988).
8. C. F. Kennel, F. V. Coroniti, *Astrophys. J.* **283**, 694 (1984).
9. S. R. Kulkarni, E. S. Phinney, C. R. Evans, G. Hasinger, *Nature* **359**, 300 (1992).
10. The observation was scheduled so that two eclipses were observed during the 43 ksec.
11. E. Høg, *et al.*, *Astron. Astrophys.* **355**, L27 (2000).
12. J. H. Taylor, J. M. Cordes, *Astrophys. J.* **411**, 674–684 (1993).
13. Q. D. Wang, Z.-Y. Li, M. C. Begelman, *Nature* **364**, 127 (1993).
14. N. Bucciantini, *Astr. Astrophys.* **387**, 1066 (2002).
15. J. Arons, *ASP Conf. Ser. 271: Neutron Stars in Supernova Remnants*, P. O. Slane, B. M. Gaensler, eds. (Astronomical Society of the Pacific, San Francisco, 2002), pp. 71+.
16. O. C. de Jager, A. K. Harding, *Astrophys. J.* **396**, 161 (1992).
17. S. Chatterjee, J. M. Cordes, *Astrophys. J.* **575**, 407 (2002).
18. We note that this spectrum differs from that used in calculating the flux in the tail region discussed in the caption to Figure 1.
19. R. Blandford, D. Eichler, *Phys. Rep.* **154**, 1+ (1987).
20. J. Arons, M. Tavani, *Astrophys. J. Supp. Series* **90**, 797 (1994).

21. M. Hoshino, J. Arons, Y. A. Gallant, A. B. Langdon, *Astrophys. J.* **390**, 454 (1992).
22. J. Arons, M. Tavani, *Astrophys. J.* **403**, 249 (1993).
23. J. H. Taylor, R. N. Manchester, A. G. Lyne, *Astrophys. J. Supp. Series* **88**, 529 (1993).
24. J. J. Hester, *et al.*, *Astrophys. J.* **448**, 240 (1995).
25. F. C. Michel, *Astrophys. J.* **431**, 397 (1994).
26. V. L. Ginzburg, S. I. Syrovatskii, *Ann. Rev. Astr. Ap.* **3**, 297 (1965).
27. B. M. Gaensler, *et al.*, *Astrophys. J.* **569**, 878 (2002).
28. M. C. Weisskopf, *et al.*, *Astrophys. J.* **536**, L81 (2000).
29. D. J. Helfand, E. V. Gotthelf, J. P. Halpern, *Astrophys. J.* **556**, 380 (2001).
30. We thank Jon Arons for useful discussions and Heath Jones for providing the Hα image. This work was supported in part by NASA through a Chandra X-ray Observatory Guest Observer grant, and by the Netherlands Organisation for Scientific Research (NWO).

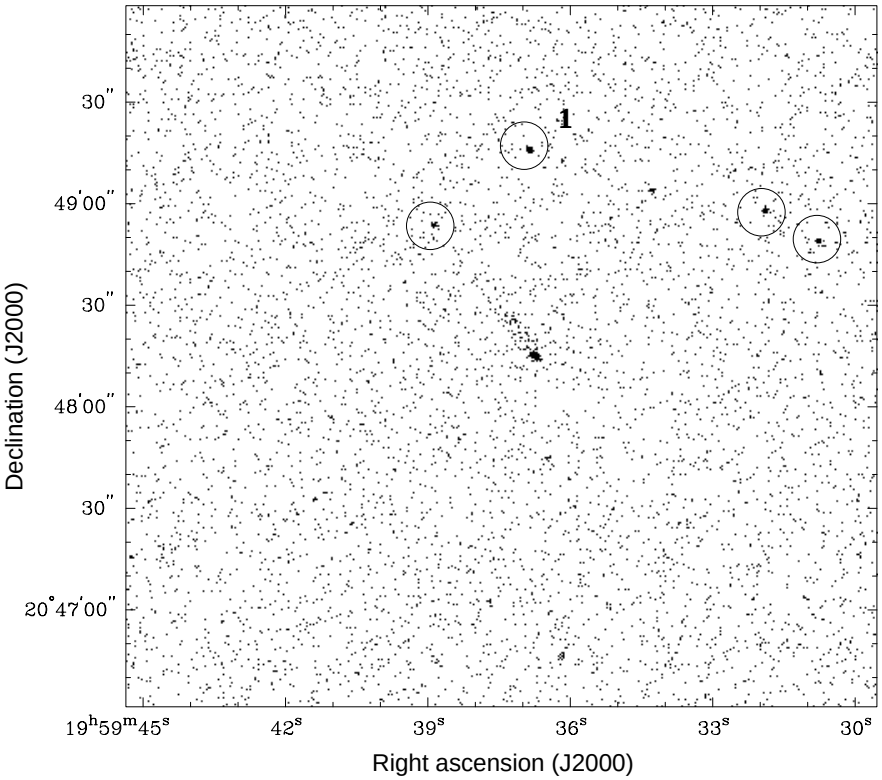

Figure 1: The full resolution *Chandra* image from the ACIS-S3 detector in the energy range 0.3–10.0 keV. The source at (J2000) RA $19^{\rm h}59^{\rm m}36\overset{\rm s}{.}75\pm0\overset{\rm s}{.}01$; Dec $+20^\circ48'15\overset{''}{.}0\pm0\overset{''}{.}1$ is coincident with the proper motion-corrected radio timing position of PSR B1957+20, RA $19^{\rm h}59^{\rm m}36\overset{\rm s}{.}75788\pm0\overset{\rm s}{.}00005$; Dec $+20^\circ48'14\overset{''}{.}8482\pm0\overset{''}{.}0006$ (*6*). Four of the next brightest x-ray sources in the field are circled and the source labeled 1 is coincident to better than $0\overset{''}{.}1$ with the Tycho II star 1628-01136-1 (*11*). In an aperture of radius $1\overset{''}{.}5$ centered on the pulsar position we detect a background corrected total of 370 ± 20 counts from the pulsar in the energy range 0.3–10.0 keV. Binning the data in energy such that each bin contains a minimum of 30 counts, we fit an absorbed power law resulting in a best fit with hydrogen column density $N_H = (1.8 \pm 0.7) \times 10^{21}$ cm^{-2}, photon index $\Gamma = 1.9 \pm 0.5$, and an unabsorbed flux density $F_{x,c} = 6 \times 10^{-14}$ ergs s^{-1} cm^{-2} (0.5–7.0 keV) corresponding to an isotropic x-ray luminosity of $L_{x,c} = 4\pi D^2 F_{x,c} = 1.6 \times 10^{31} D_{1.5}$ ergs s^{-1} (0.5–7.0 keV), where $D_{1.5} = D/(1.5{\rm kpc})$ is the pulsar distance as derived from its dispersion measure (*12*). Counts in the tail region were summed in a $16'' \times 6''$ box enclosing the tail and aligned with the proper motion direction. After background correction, we detect a total of 82 ± 9 counts from the tail region. Again fitting an absorbed power law and assuming that the N_H and Γ are similar to the values above we derive an unabsorbed flux density $F_{x,t} = 9 \times 10^{-15}$ ergs s^{-1} cm^{-2} (0.5–7.0 keV).

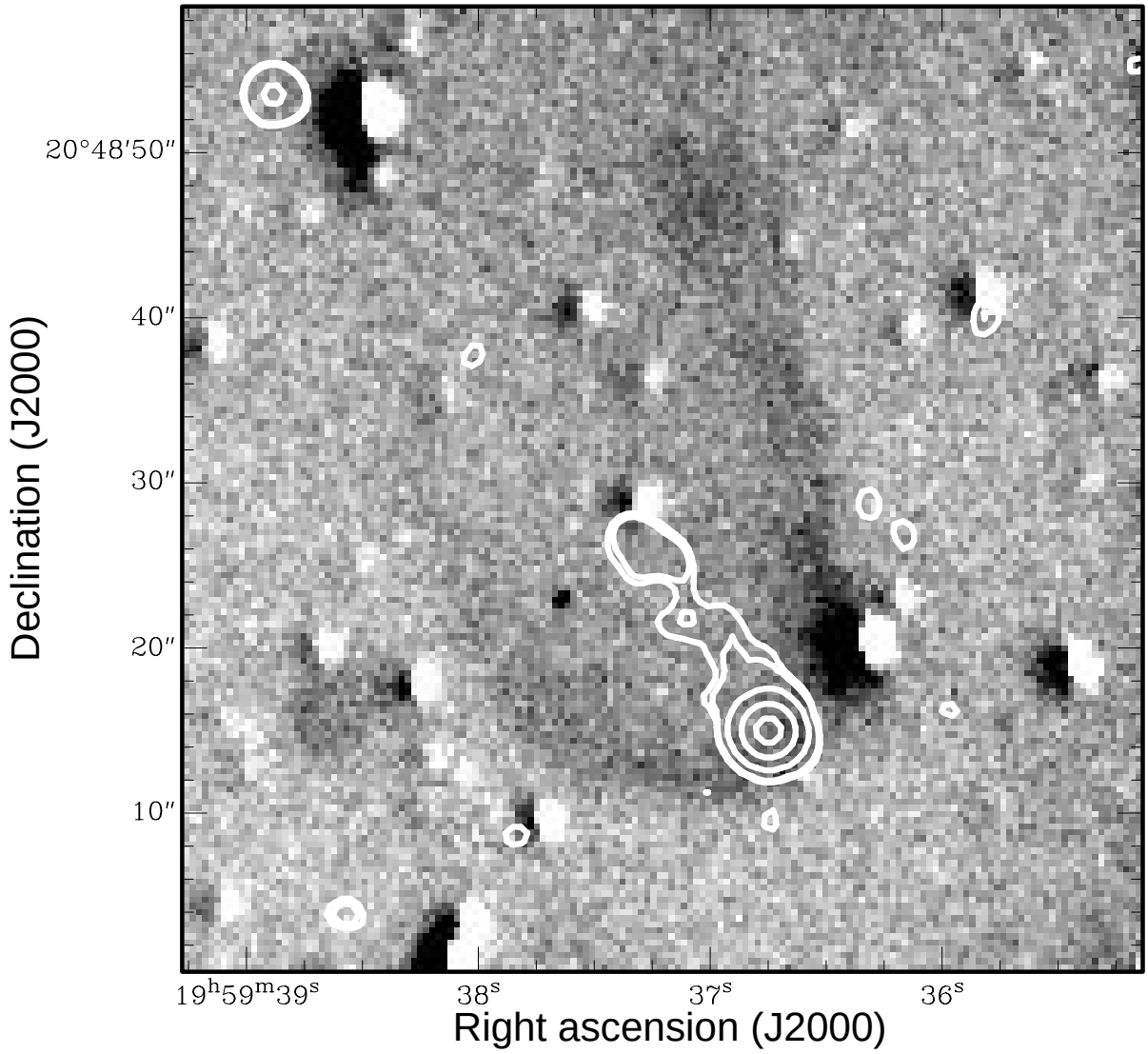

Figure 2: The same *Chandra* data as shown in Figure 1, smoothed to a resolution of 5″ (contours) and overlaid on an Hα image obtained from Taurus Tunable Filter service mode observations on the Anglo Australian Telescope on 2000 Aug 3. The images were aligned to within $\sim$0.″2 through use of USNO 2.0 stars. The x-ray tail is located well inside the boundaries of the Hα emission and also close to its symmetry axis. The x-ray contour levels are shown at 0.9, 1.2, 5.3, 35.0 and 78.8% of the peak x-ray surface brightness. The optical residuals correspond to incompletely subtracted stars. No optical counterpart was found to the x-ray source associated with the contours located in the northeastern corner of the field on a Digitized Sky Survey image.

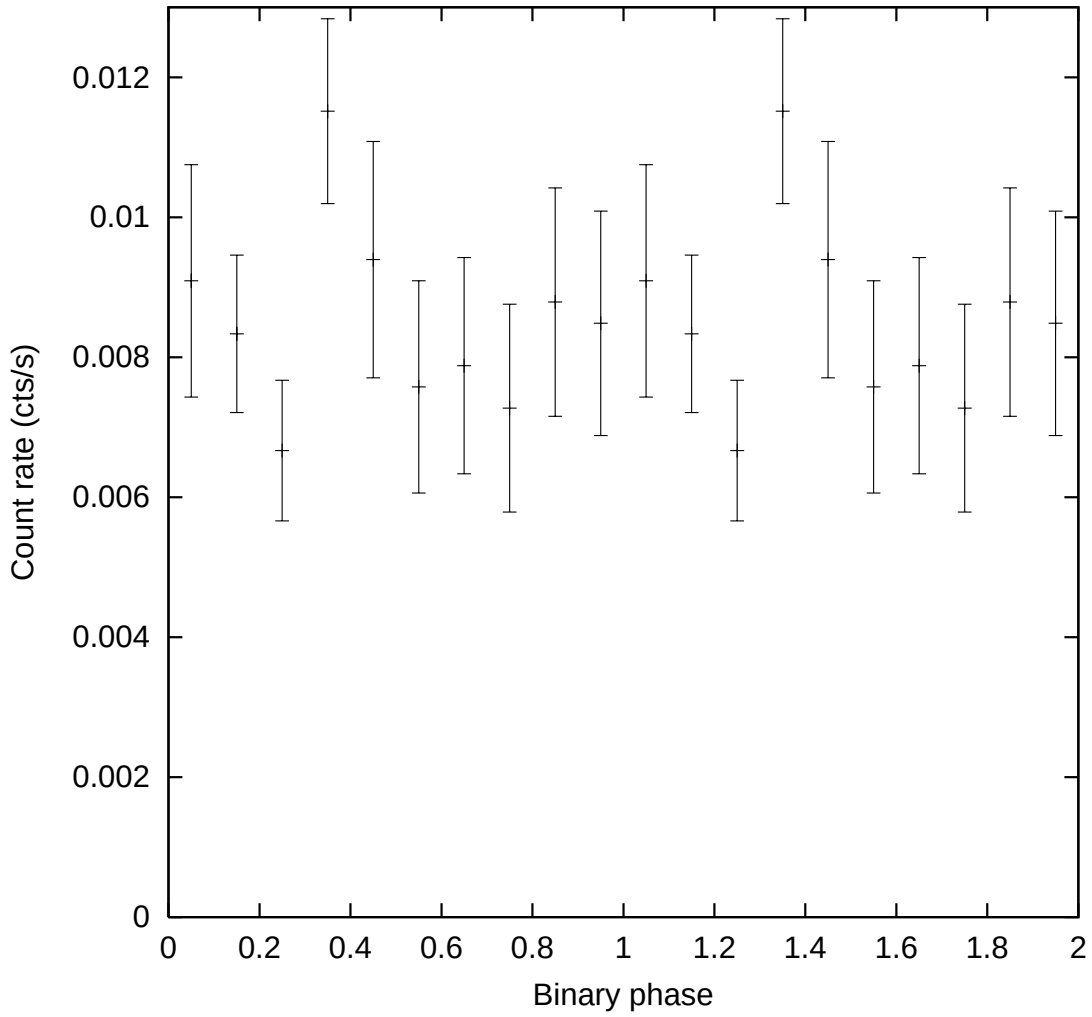

Figure 3: The light curve of the x-ray emission (0.3–10.0 keV) from the point source associated with PSR B1957+20 folded through use of the known orbital ephemeris (D. J. Nice, private communication, 2001). The errorbars correspond to one-sigma Poissonian errors. Radio eclipse occurs at orbital phase 0.25. The mean count rate, excluding phases in the range 0.15–0.35 where variations in the x-ray flux are expected, is (8.4 ± 0.8) cts ksec^{-1}. Orbital phase bins 0.25 and 0.35 each correspond to a total observing time of 6600s, and thus we expect to measure 55 counts in each of these phase bins. Using Poisson statistics, the 76 counts detected at phase 0.35 deviate from the expected 55 counts with 99% confidence. Scattering and/or absorption of the x-ray emission could reduce the degree of modulation at either phase 0.15 or 0.35. Taking into account either possibility, the chance probability for the observed variation at phase 0.35 is 2%. A decrease in the count rate is predicted at orbital phase 0.25 and the 44 counts we detect in this phase bin have a 4% chance probability of being drawn from a steady flux distribution.